

Robotica

<http://journals.cambridge.org/ROB>

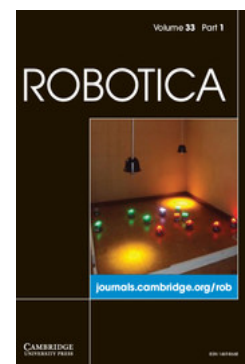
Additional services for **Robotica**:

Email alerts: [Click here](#)

Subscriptions: [Click here](#)

Commercial reprints: [Click here](#)

Terms of use : [Click here](#)



The shape control of tentacle arms

Mircea Ivanescu, Nirvana Popescu and Decebal Popescu

Robotica / Volume 33 / Issue 03 / March 2015, pp 684 - 703

DOI: 10.1017/S0263574714000885, Published online: 09 April 2014

Link to this article: http://journals.cambridge.org/abstract_S0263574714000885

How to cite this article:

Mircea Ivanescu, Nirvana Popescu and Decebal Popescu (2015). The shape control of tentacle arms. Robotica, 33, pp 684-703 doi:10.1017/S0263574714000885

Request Permissions : [Click here](#)

The shape control of tentacle arms

Mircea Ivanescu^{†*}, Nirvana Popescu^{††} and
Decebal Popescu^{††}

[†]*Department of Mechatronics, University of Craiova, Craiova, Romania*

^{††}*Department of Computer Science, University Politehnica Bucharest, Bucharest, Romania*

(Accepted March 9, 2014. First published online: April 9, 2014)

SUMMARY

The paper discusses the shape control problem related to a class of hyper-redundant robot arms with continuum elements, i.e. tentacle arms. A spatial weighted technique for sensor measurements is used in order to facilitate the parameter estimation. The paper focuses on the shape control by using the curvature gradient a constant parameter along the segment arm. The conditions that ensure a constant curvature gradient for a class of tentacle arms characterized by elastic backbone are determined. A sensor network distributed along the robot arm is used for the shape control. The main parameters of the arm shape, curvature and curvature gradient or “shape” Jacobian for the control problem are estimated. Two measuring systems are used: a) a distributed angle sensor network and b) a curvature sensor placed at the end of the arm segment. The stability analysis and the resulting controllers are obtained using the concept of boundary geometric control and the weighted state control methods. The shape control algorithms for dynamic models with uncertain components are proposed. Numerical simulations and experimental results illustrate the effectiveness of the above mentioned algorithms.

KEYWORDS: Redundant manipulators; Robot dynamics; Control of robotic systems; Mechatronic systems; Sensor or actuator design.

1. Introduction

The paper aims to implement a control algorithm for a tentacle arms by using a spatial weighted technique for sensor measurements. Tentacle arms represent a class of hyper-redundant robots, continuum models, which can reach any position and orientation in space. These arms are mechanical structures with continuum elements described by distributed parameter models. The control of these systems is very complex and literature abounds in studies addressing this topic. Robinson and Davies¹ introduced the notion of continuum elements. In Chirikjian,^{2–5} Gragnone,^{6,7} the kinematic models were analysed, based on a “backbone curve” that captures the robot macroscopic geometric features. In Mochiyama,⁸ the problem of controlling the shape of a robot with two-degree-of-freedom joints was also investigated using spatial curves. A controller for continuum robots was developed by using neural network feed-forward components in Braganza.⁹ Other researchers derived a new kinematic model by using differential geometry, Walker,¹⁰ proposed a real-time controller for continuum robots, Jones¹¹ and Rucker¹³ developed new hyper-redundant configurations. In Kapadia¹² a sliding controller was proposed for extensible robots and Gragnone¹⁴ studied the manipulability of continuum robots. The control problem of a class of continuum arms that perform the grasping function by coiling is also discussed in Ivanescu.¹⁵ A frequency stability criterion for the grasping control problem is advanced in Ivanescu.¹⁶ Several biomimetic robotic prototypes with undulatory actuation have been developed in La Spina,¹⁷ KeJun,¹⁸ Camarillo.³² Continuum robots with multiple, concentric, precurved elastic tubes were analysed and discussed in Rucker,¹⁹ Bailly,²⁰ Bajo,²¹ Due to their many degrees of freedom, tentacle robots are potentially superior with regard to operations in highly constrained and unusual environments or to complex operations of grasping. In the case of these applications, local

* Corresponding author. Email: al-ivanescu@robotics.ucv.ro

sensor-based motion planning schemes are vital. In Choset²⁴ a local sensor based planning method is extended for hyper redundant robots using the term partial shape modification. The local sensor based planning algorithm for these arms was developed in Rucker¹⁹ and Shugen Ma.²⁵ A measuring system of the curvature on the boundary, an observer and a control algorithm is proposed in Ivanescu.¹⁶ These papers are premised by the idea that the sensors provide perfect information about the environment. Hirose²³ implemented an active cord mechanism which used tactile sensors to guide its motion. Several other theories have been published in Jones²⁶ and Fareh.²⁷

Almost all previous approaches do not address the arm orientation and approximate positional kinematics, or solve them only for limited kinematic models, which constrain the performance of continuum robot hardware to a small number of classes of shapes and motions, restricting their potential applicability. For example, Jones²⁶ uses the Denavit-Hartenberg method presupposing that the arm bends with constant curvature. Hirose *et al.* designed the serpenoid curve, which closely matches the kinematics of a snake's body in 2-D as it crawls across the ground (Hirose³¹). Fahimi³⁰ chooses a curve—an arc of a circle—which closely matches the kinematics of continuum robots. Likewise, Kapadia³² proposes the curvature and length of the arm as main parameters for a hyper redundant arm with extensible length, Webster,³³ analyses continuum robots by constant curvature techniques, Hannan³⁴ introduces a real time procedure for continuum robot estimation and Sareh³⁶ focuses on the parameters of biomimetic artificial structures.

All these research paper shighlight the complexity of control problems as well as the difficulty in implementing feedback controllers and compensators. The difficulty is determined by the dynamic models expressed by partial differential equations (PDE) and by the observability problems in distributed parameter systems. Geometric control has proved to be very successful asacontrol approach to the PDE system and successful applications are reported in literature, Shang,²⁸ Maidi.²⁹ Designing a control law based on geometric control theory presents the advantage that the distributed model can be used in control design with no approximation.

This paper focuses on the shape control problem of tentacle arms with continuum elements. It discusses the shape control by using a spatial weight technique for sensor measurements in order to facilitate the parameter estimation. A sensor network, distributed along the robot arm, is used for shape control. The main parameters of the arm shape, as curvature and curvature gradient or “shape” Jacobian for the control problem can be easily estimated. Two measuring systems are used: a) a distributed angle sensor network and b) a curvature sensor placed at the end of the arm segment. Whereas numerous papers (see above) propose control solutions mainly based on the orientation angles (θ, q) , our control methodology underlies the curvature gradient $\kappa' = \frac{d\kappa}{ds}$ defined as “state variable” associated with the arm. The conditions that ensure a constant curvature gradient for a class of tentacle arms characterized by elastic backbones are established. The proposed algorithms provide a simpler control solution with respect to the conventional solutions based on orientation angles. The stability analysis and the resulting controllers are obtained using the concept of boundary geometric control and a weighted state control method. The paper is structured as follows: Section 2 presents model parameters, Section 3 analyses the mathematical model, Section 4 discusses the control problem, Section 5 verifies the control laws by computer simulation, Section 6 presents experimental results and Section 7 is dedicated to the conclusions.

2. Model Parameters

We consider a tentacle arm as presented in Fig. 1(a). This arm consists of a chain of segments (Fig. 1b), each segment being able to any position and orientation in space.

The essence of the arm is the backbone curve Γ (Fig. 2). The independent parameter s is related to the arc-length from the origin of the curve Γ , $s \in \Omega$, $\Omega = [0, l]$, where l is the length of the inextensible arm. The position of a point s on the curve Γ is defined by the position vector $r = r(s)$, $s \in [0, l]$ and the orientation is given by two continuum angles $\theta(s)$ and $q(s)$, where $\theta, q \in (L_2(\Omega) \times L_2(\Omega))$. We used a parameterization of the curve Γ based upon two “continuous angles” $\theta(s)$ and $q(s)$, (Fig. 3), (Chirikjian^{2,3}), (Gravagne^{6,7}), and denote the orientation vector by ω ,

$$\omega(s) = \begin{bmatrix} \theta(s) \\ q(s) \end{bmatrix}. \quad (2.1)$$

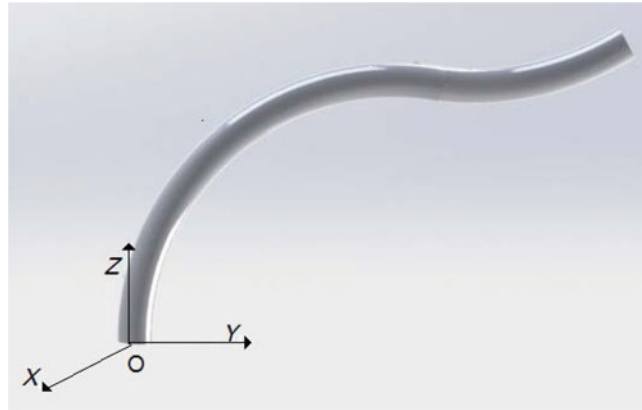
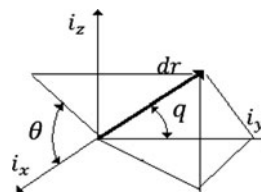


Fig. 1. A tentacle arm.



Fig. 2. The arm segment.

Fig. 3. Definition of angles θ , q .

At each point $r(s)$, the robot's orientation is given by a right-handed orthonormal basis vector $\{i_x, i_y, i_z\}$ and its origin coincides with the point $r = r(s)$.

$$r = \begin{bmatrix} x \\ y \\ z \end{bmatrix} = \begin{bmatrix} \int_0^s \cos \theta \sin q ds \\ \int_0^s \cos q ds \\ \int_0^s \sin \theta \sin q ds \end{bmatrix}. \quad (2.2)$$

The orientation or the “shape” of the curve can be also defined by the curvature determined by the two angles,

$$\kappa_\theta = \frac{d\theta}{ds}. \quad (2.3)$$

$$\kappa_q = \frac{dq}{ds}. \quad (2.4)$$

We denote “the curvature gradient” by $\kappa'_\theta, \kappa'_q$,

$$\kappa'_\theta = \frac{d\kappa_\theta}{ds}, \quad (2.5)$$

$$\kappa'_q = \frac{d\kappa_q}{ds}. \quad (2.6)$$

Let κ, κ' be the curvature and curvature gradient vectors,

$$\kappa = (\kappa_\theta, \kappa_q)^T, \quad (2.7)$$

$$\kappa' = (\kappa'_\theta, \kappa'_q)^T. \quad (2.8)$$

3. A Dynamic Model

The dynamic model of this arm with continuum elastic backbone is derived from the Hamiltonian principle (Gravagne⁷) as

$$I_\rho \ddot{\omega} = EI \omega_{ss} - B \dot{\omega} + C \omega + h(\omega, \dot{\omega}), \quad (3.1)$$

where $\omega = \omega(t, s)$, $\omega = (\theta, q)^T$, $s \in \Omega$, $\dot{\omega} = \partial \omega / \partial t$, $\omega_s = \partial \omega / \partial s$, I_ρ is the rotational inertial density matrix, $I_\rho = \text{diag}(I_{\rho\theta}, I_{\rho q})$, EI is the bending stiffness matrix, $EI = \text{diag}((EI)_\theta, (EI)_q)$, C characterizes the elastic behaviour, $C = \text{diag}(c_\theta, c_q)$, B is the equivalent damping matrix of the arm, $B = \text{diag}(b_\theta, b_q)$ and h represents the nonlinear component vector determined by the gravitational and Coriolis components, $h(\omega, \dot{\omega}) = (h_1(\omega, \dot{\omega}), h_2(\omega, \dot{\omega}))^T$. The initial and boundary conditions are

$$\omega(0, s) = \omega_0(s), \quad (3.2)$$

$$EI \omega_s(t, l) = \tau(t), \omega_s(t, 0) = 0, \quad (3.3)$$

where τ is the equivalent moment generated at the end of the arm segment, $\tau = (\tau_\theta, \tau_q)^T$. We assumed that the effect of the shear and axial deformations were neglected for this thin arm. The state of the system is defined by the vector $\vec{\omega} = (\omega, \dot{\omega}) \in (H^1(\Omega) \times L_2(\Omega))$, (L, H represent the standard notations for Hilbert and Sobolev spaces) and the input is represented by the moment $\tau(t)$ at the boundary of the arm. We assume that the nonlinear term $h(\omega, \dot{\omega})$ verifies the inequality

Assumption 1:

$$||h_i(\cdot, t)|| \leq M ||\vec{\omega}(\cdot, t)||, \quad i = 1, 2. \quad (3.4)$$

we consider a desired state $\omega^d(s)$, $\omega^d \in L_2(0, l)$, that satisfies (3.1) with boundary conditions (3.3) and which corresponds to the desired curvature $\kappa_d = (\kappa_{\theta d}, \kappa_{q d})^T$ in the task-space. We denote by

$$\Delta \omega(t, s) = \omega^d(s) - \omega(t, s). \quad (3.5)$$

the error variable, $\Delta \omega \in L_2(0, l)$.

Problem A. The measuring of curvature is obtained by a distributed angle sensor network with $\xi = (\xi_1, \xi_2, \dots, \xi_N)^T$ (Fig. 4a). We consider that the position measuring of a tentacle segment is

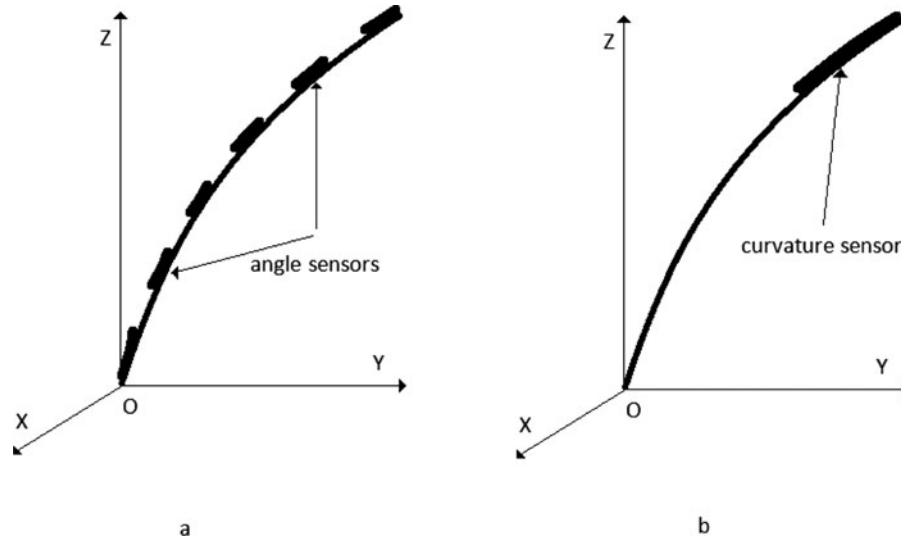


Fig. 4. (a) Angle sensor network. (b) Curvature sensor.

obtained by electro-active polymer sensor network that are placed on the surface, at the location, $\xi \in \Omega_s$, $\Omega_s \subset \Omega$, where Ω_s denotes the domain of permissible sensor locations, with the boundaries $\partial\Omega_s$, $\Omega_s = \cup_{si} \Omega_s^i$,

$$\Omega_{si} = \left(\xi_i - \frac{\rho}{2}, \xi_i + \frac{\rho}{2} \right], i = 1, 2, \dots, N-1 \quad (3.6)$$

$$\Omega_{s0} = \left[0, \frac{\rho}{2} \right], \Omega_{sN} = \left(l - \frac{\rho}{2}, l \right]$$

We denote the vector of the sensor positions by

$$\xi = (\xi_1, \xi_2, \dots, \xi_N)^T \quad (3.7)$$

Definition 1. The ξ Weighted State Vector (ξ – WSV) with respect to a sensor network $\xi = (\xi_1, \xi_2, \dots, \xi_N)^T$ is the weighted geometric mean of the orientation vector (2.1),

$$\tilde{\omega}^\xi(t) = \frac{1}{\overline{\chi}(\xi)} \int_0^l \chi(s, \xi) \omega(t, s) ds, \quad (3.8)$$

$\tilde{\omega}^\xi \in C^2$, where

$$\chi(s, \xi) = \sum_{j=1}^N \chi^j(s, \xi_j), \quad (3.9)$$

$$\overline{\chi}(\xi) = \int_0^l \chi(s, \xi) ds, \quad (3.10)$$

and $\chi^i(s, \xi_i)$ is the spatial weighting function of the sensor ξ_i . $\chi^i \in L_2(0, l)$, $i = 1, 2, \dots, N$. We consider the weighting function (Fig. 5),

$$\chi^i(s, \xi_i) = \begin{cases} A \sin \left(j \frac{\pi}{\rho} \left(s - \xi_i + \frac{\rho}{2j} \right) \right), & |s - \xi_i| \leq \rho/2j \\ 0, & |s - \xi_i| \geq \rho/2j \end{cases} \quad (3.11)$$

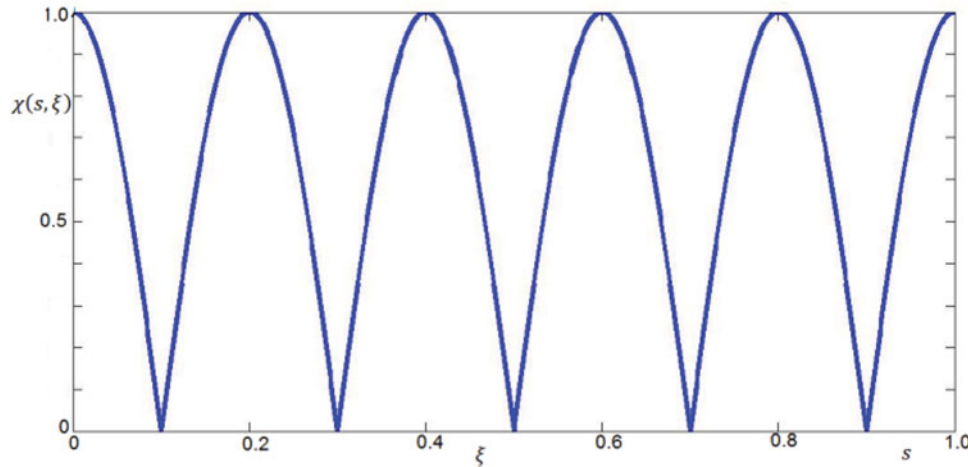


Fig. 5. The weighting functions for a sensor network ($A = 1$, $\rho = 0.2$).

where ξ_i represents the sensor position, A is the magnitude and ρ defines the function characteristic. This function is an eigenfunction of the spatial operator $\frac{d^2}{ds^2}$,

$$\frac{d^2 \chi^i(s, \xi_i)}{ds^2} = -\Lambda_j \chi^i(s, \xi_i) \quad (3.12)$$

$$\chi^i(s = \partial\Omega_s, \xi_i) = 0; \frac{d\chi^0}{ds}(0, \xi_0) = 0; \frac{d\chi^N}{ds}(l, \xi_N) = 0; \quad (3.13)$$

and Λ_j can be selected as,

$$\Lambda_j = j^2 \frac{\pi^2}{\rho^2}, \quad j = 1, 2, \dots$$

In terms of the Definition 1, the error variable $\Delta\omega$ becomes,

$$\tilde{\Delta}\omega^\xi(t) = \frac{1}{\chi(\xi)} \int_0^l \chi(s, \xi) \Delta\omega(t, s) ds \quad (3.14)$$

and the dynamic Eq. (3.1) can be rewritten as,

$$\begin{aligned} \int_0^l \frac{EI}{\chi(\xi)} \chi(s, \xi) I_\rho \Delta\ddot{\omega}(t, s) ds &= \int_0^l \frac{EI}{\chi(\xi)} \chi(s, \xi) \Delta\omega_{ss}(s) ds - \int_0^l \frac{B}{\chi(\xi)} \chi(s, \xi) \Delta\dot{\omega}(s) ds \\ &+ \int_0^l \frac{C}{\chi(\xi)} \chi(s, \xi) \Delta\omega(s) ds + \int_0^l \frac{1}{\chi(\xi)} \Delta\chi(s, \xi) h(\omega) ds \end{aligned} \quad (3.15)$$

or integrating by parts the first term and using the boundary conditions (3.3), (3.13), we have,

$$I_\rho \ddot{\Delta}\omega^\xi(t) + B \dot{\Delta}\omega^\xi(t) + (EI\Lambda_j - C) \tilde{\Delta}\omega^\xi(t) - \tilde{\Delta}h = \frac{\chi(l, \xi)}{\tilde{\chi}(\xi)} \Delta\tau \quad (3.16)$$

with initial conditions,

$$\tilde{\Delta}\omega^\xi(0) = 0 \quad (3.17)$$

where

$$\Delta \tilde{h} = \frac{1}{\chi(\xi)} \int_0^l \chi(s, \xi) (h - h^d) ds \quad (3.18)$$

$$\tau = \tau^d - \Delta \tau \quad (3.19)$$

and τ^d, h^d are defined on the desired trajectory.

Lemma 1. If the spatial weighted error $\tilde{\Delta} \omega^\xi(t)$ converges to zero, the system trajectory $\omega(t, s)$ converges to the desired position $\omega^d(s), s \in \Omega$.

Proof. For the domain Ω_{si} , $\tilde{\Delta} \omega^\xi(t)$ will be,

$$\tilde{\Delta} \omega^\xi(t) = \frac{1}{\chi(\xi)} \int_{\xi^i - \frac{\rho}{2j}}^{\xi^i + \frac{\rho}{2j}} \chi^i(s, \xi_i) (\omega^d(s) - \omega(t, s)) ds \quad (3.20)$$

Clearly, from (3.11), $(\chi^i(s, \xi_i) > 0, s \in (\xi^i - \frac{\rho}{2j}, \xi^i + \frac{\rho}{2j}))$, if $\lim_{t \rightarrow \infty} \tilde{\Delta} \omega^\xi(t) = 0$ yields $\lim_{t \rightarrow \infty} \omega(t, s) = \omega^d(s)$ and by virtue of the continuity of ω , this result can be verified on the boundary $s = (\xi^i + \frac{\rho}{2j})$. We can conclude that the convergence to zero of the error $\tilde{\epsilon}^\xi$ in the domain $(\xi^i - \frac{\rho}{2j}, \xi^i + \frac{\rho}{2j})$ determines the convergence of the trajectory ω to the desired ω^d . Now, we can extend this result to the global domain, $\Omega = \cup_{si} \Omega_{si}, i = 0, 1, \dots, N$.

$$\lim_{t \rightarrow \infty} \omega(t, s) = \omega^d(s), s \in \Omega \quad (3.21)$$

Remark. The system stability with respect to $\tilde{\Delta} \omega^\xi$ ensures stability with respect to $\omega(t, s)$

$$\lim_{t \rightarrow \infty} \Delta \omega(t, s) = 0, s \in \Omega, \quad (3.22)$$

Problem B. The measuring of curvature is obtained by a curvature sensor placed at the end of the segment ($\xi = l$) (Fig. 4b).

Assumption 2: The elastic components have higher values than the inertial and viscous friction components, (Comp/Reader: Please match all equations with the original paper.)

$$\|EI \widetilde{\Delta} \omega^\xi + C \widetilde{\Delta} \omega^\xi\| > \|I_\rho \ddot{\widetilde{\Delta} \omega^\xi}\| \quad (3.23)$$

$$\|EI \widetilde{\Delta} \omega^\xi + C \widetilde{\Delta} \omega^\xi\| > \|B \dot{\widetilde{\Delta} \omega^\xi}\| \quad (3.24)$$

This assumption is normal for this light and thin class of manipulators.

Equation (3.16) represents the dynamic model of the arm segment with respect to the angle parameters $\omega(t, s)$. A similar model can be obtained if the curvature gradient vector κ' is used and the arm state is defined as $(\kappa', \dot{\kappa}')$.

In terms of Definition 1, we have the weighted curvature gradient vector,

$$\tilde{\kappa}'^\xi = \frac{1}{\chi(\xi)} \int_0^l \kappa' \chi(s, \xi) ds \quad (3.25)$$

Integrating by parts the second term in (3.15) and using the boundary conditions (3.3), (3.13), we have,

$$\int_0^l \frac{EI}{\chi(\xi)} \chi(s, \xi) \omega_{ss}(t, s) ds = \frac{EI}{\chi(\xi)} \int_0^l \chi_{ss}(s, \xi) \omega(t, s) ds + \frac{\chi(l, \xi)}{\chi(\xi)} \tau^s(t) \quad (3.26)$$

or,

$$EI \tilde{\kappa}'^\xi = -\Lambda_j EI \tilde{\omega}^\xi + \frac{\chi(l, \xi)}{\chi(\xi)} \tau^s \quad (3.27)$$

where the variables t, s were omitted. Now, differentiating, we obtain

$$EI \Delta \tilde{\kappa}'^\xi = -\Lambda_j EI \Delta \tilde{\omega}^\xi + \frac{\chi(l, \xi)}{\chi(\xi)} \Delta \tau^s. \quad (3.28)$$

Taking into account the conditions (3.23) and (3.24), eq (3.16) can be rewritten in terms of κ'^ξ ,

$$EI \Delta \tilde{\kappa}'^\xi + C \Delta \tilde{\omega}^\xi + \Delta \tilde{h}^\xi = 0 \quad (3.29)$$

From (3.28), (3.29) yields,

$$\Delta \tilde{\kappa}'^\xi = (EI)^{-1} (C - \Lambda_j EI)^{-1} \left(\frac{\chi(l, \xi)}{\chi(\xi)} C \Delta \tau^s - \Lambda_j EI \Delta \tilde{h}^\xi \right) \quad (3.30)$$

Assumption 3: The boundary control verifies the inequality,

$$\|\Delta \tau^s\| > \Lambda_j \frac{\overline{\chi(\xi)}}{\chi(l, \xi)} \frac{(EI)^*}{c^*} \|\Delta h^\xi\| \quad (3.31)$$

where $(EI)^* = \|EI\|$, $c^* = \|C\|$.

Lemma 2 If the boundary control satisfies the condition (3.31), the weighted curvature gradient vector is constant along the arm.

Proof By using (3.31), from (3.30) we obtain

$$\Delta \tilde{\kappa}'^\xi \cong (EI)^{-1} (C - \Lambda_j EI)^{-1} \frac{\chi(l, \xi)}{\chi(\xi)} C \Delta \tau^s \quad (3.32)$$

It turns out that κ'^ξ depends solely on the torque, it is constant along the tentacle segment actuated by a torque τ^s .

Remark 1. If we assume that

$$C > \Lambda_j EI \quad (3.33)$$

the relation (3.32) becomes

$$\Delta \tilde{\kappa}'^\xi \cong (EI)^{-1} \frac{\chi(l, \xi)}{\chi(\xi)} \Delta \tau^s \quad (3.34)$$

This result is similar to the classical formula of the curvature gradient for the beams (Beer³⁸) where

$$\tilde{\kappa}' = (EI)^{-1} \tau^s \quad (3.35)$$

Remark 2. From (3.25), we have,

$$\tilde{\kappa}'^\xi = \frac{1}{\chi(\xi)} \int_0^l \kappa' \chi(s, \xi) ds \cong \kappa' \quad (3.36)$$

Remark 3. The curvature and orientation vector κ, ω can be easily evaluated as ((2.3)–(2.6)),

$$\kappa(s) \cong \int_0^s \tilde{\kappa}'^\xi ds' + \kappa(0) \quad (3.37)$$

$$\omega(s) \cong \int_0^s \left(\int_0^{s'} \kappa'^{\xi} ds' + \kappa(0) \right) ds + \omega(0) \quad (3.38)$$

where $\kappa(0)$, $\omega(0)$ represent the boundary ($s = 0$) curvature and orientation.

Remark 4. Based on the kinematic relations (2.3)–(2.8), the arm shape (curvature) is proposed to be evaluated, with respect the desired curvature ($\kappa_{\theta d}$, κ_{qd}), as

$$\eta(\kappa_{\theta}, \kappa_q) = \begin{bmatrix} \eta_1 \\ \eta_2 \end{bmatrix} = \frac{1}{2} \begin{bmatrix} (\kappa_{\theta} - \kappa_{\theta d})^2 \\ (\kappa_q - \kappa_{qd})^2 \end{bmatrix} \quad (3.39)$$

where $\eta \in C^2$ and κ_{θ} , κ_q are defined by the forward kinematics of the arm (2.3), (2.4). We have chosen this (2×1) vector as a task space function in order to facilitate the construction of a (2×2) „shape” Jacobian matrix.

We define by

$$\Delta\eta = \eta(\kappa_{\theta}, \kappa_q) - \eta(\kappa_{\theta d}, \kappa_{qd}) \quad (3.40)$$

where $\eta(\kappa_{\theta d}, \kappa_{qd}) = 0$. The variable $\Delta\eta$ in (3.40) represents the curvature error vector.

From (2.3)–(2.6), (2.9), the differential relationships between the arm orientation and the arm parameters can be calculated as

$$\Delta\eta = J^{\xi}(\tilde{\omega}^{\xi})\Delta\tilde{\omega}^{\xi} \quad (3.41)$$

where J^{ξ} is the “shape” Jacobian, defined with respect to the variables $\tilde{\omega}^{\xi}$. This shape or orientation Jacobian is represented by a diagonal (2×2) matrix with components that do not impose the computational difficulties (See Appendix 1).

From *Lemma 2* and *Remark 1*, κ' is constant along the arm segment, $\kappa' = \kappa'(t)$. Considering the initial conditions $\kappa(0) = 0$, $\omega(0) = 0$ in (3.37), (3.38) and substituting them in (3.1), we have

$$\frac{1}{2}s^2 I_{\rho} \ddot{\kappa}'(t) = EI\kappa'(t) - \frac{1}{2}s^2 B\dot{\kappa}'(t) + \frac{1}{2}s^2 C\kappa'(t) + h(\kappa', \dot{\kappa}', s), \quad s \in [0, l] \quad (3.42)$$

with the initial condition

$$\kappa'(0) = \kappa'_0. \quad (3.43)$$

The dynamics of the arm segment in terms of $(\kappa', \dot{\kappa}')$ presupposes the evaluation of the curvature and of the curvature gradient at the end of the segment, $s = l$,

$$\frac{1}{2}l^2 I_{\rho} \ddot{\kappa}'(t) = EI\kappa'(t) - \frac{1}{2}l^2 B\dot{\kappa}'(t) + \frac{1}{2}l^2 C\kappa'(t) + h(\kappa', \dot{\kappa}', l), \quad (3.44)$$

$$\kappa(t, l) = \kappa(t, 0) + \kappa'(t)l, \quad (3.45)$$

$$\kappa(t, l) = (EI)^{-1}\tau(t). \quad (3.46)$$

Considering the boundary condition $\kappa(t, 0) = 0$, taking into account the (3.45), (3.46), the dynamic model (3.44) becomes

$$\frac{1}{2}l^2 I_{\rho} \ddot{\kappa}'(t) = -\frac{1}{2}l^2 B\dot{\kappa}'(t) + \frac{1}{2}l^2 C\kappa'(t) + h(\kappa', \dot{\kappa}', l) + \frac{1}{l}\tau(t). \quad (3.47)$$

with the initial condition (3.43).

4. Control Algorithm

Definition 2. The shape control system is stable if

$$\lim_{t \rightarrow \infty} \Delta \eta(t) = 0 \quad (4.1)$$

In terms of this definition we can synthesize a controller that guarantees stability in the closed loop system.

Problem A. The measuring of the curvature is obtained by a distributed angle sensor network.

Theorem 1. A closed loop control of the system (3.1)-(3.3) is asymptotically stable if the control law is

$$\Delta \tau^\xi(t) = \frac{\overline{\chi(l, \xi)}}{\chi(l, \xi)} \left(-K_1 \int_0^l \chi(s, \xi) (\omega^d(s) - \omega(t, s)) ds - K_2 \int_0^l \chi(s, \xi) (-\dot{\omega}(t, s)) ds \right) \quad (4.2)$$

provided the arm does not achieve a singular configuration, where K_1, K_2 are the positive control coefficients that satisfy the following conditions,

$$(B - \alpha I + K_2) > 0 \quad (4.3)$$

$$\alpha (B - \alpha I + K_2) ((EI\Lambda - C) + K_1) - \frac{1}{4} (\alpha B - (MI - K_1) - \alpha (MI - K_2))^2 > 0 \quad (4.4)$$

and α is a positive constant that satisfies (4.6).

Proof. See Appendix 2.

Problem B. The measuring of the curvature is obtained by a curvature sensor placed at the end of the sement.

Theorem 2. A closed control of the system (3.47) with initial condition (3.43) is asymptotic stable if the control law is

$$\Delta \tau(t) = -K_1(\kappa_d(l) - \kappa(t, l)) + K_2 \dot{\kappa}(t, l) \quad (4.5)$$

provided the arm does not achieve a singular position, where K_1, K_2 are the positive control coefficients that satisfy the following conditions,

$$\left(\frac{l}{2} B - \frac{l}{2} \alpha I_\rho + K_2 - MI \right) > 0 \quad (4.6)$$

$$\alpha \left(\frac{l}{2} B - \frac{l}{2} \alpha I_\rho + K_2 - MI \right) \left(\frac{l}{2} C - M + K_1 \right) - \alpha (-lC + K_1) \left(\frac{l}{2} B + K_2 \right) > 0 \quad (4.7)$$

and α is a positive constant that satisfies

$$4C > \alpha^2 I_\rho. \quad (4.8)$$

Proof. See Appendix 3.

5. Numerical Simulations

Consider a 2-D (XOZ) dynamic model of a vertical tentacle arm described by (3.1), where the state is defined by $(\theta, \dot{\theta})$, with the length of the arm, $l = 1$ m, the rotational inertial density is $I_\rho = 0.001$ kg m², the bending stiffness $EI = 0.1$ Nm³, the viscous coefficient is $b_\theta = 0.06$ Nms/rad, and the elastic coefficient is $c_\theta = 8.5 \cdot 10^2$ N/rad. These constants are scaled to realistic ratios for the long thin arm. The initial and boundary conditions are: $\theta_0(s) = 0$, $\theta_s(t, 0) = 0$; $EI\theta_s(t, l) = \tau$, where τ is

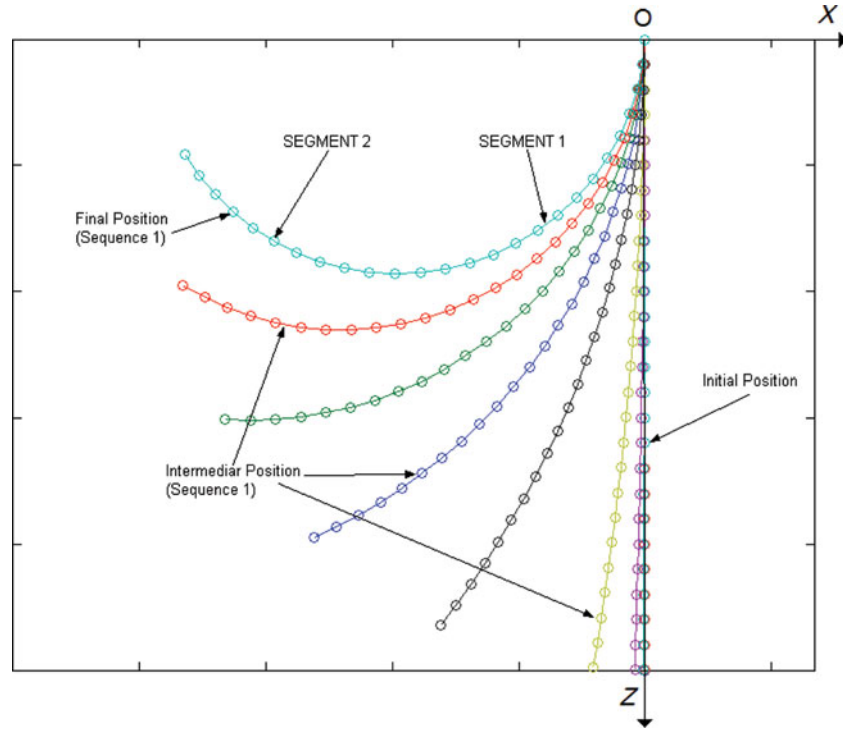


Fig. 6. The arm motion during the Sequence 1 (Problem A).

the torque applied to the top of the arm ($s = l$). We consider that the uncertain term $h(\theta)$ is defined by the gravitational components, $h(s) = \frac{\partial V_P}{\partial \theta} = \rho_b g A \int_0^s \cos(\theta) ds$, where V_P is the gravitational potential, ρ_b is the linear density, g is the gravitational acceleration and A is the section area. For the characteristic values of these parameters, $\rho_b = 0.8 \text{ kg/m}$, $g = 10 \text{ m/s}^2$, $A = 4 \cdot 10^{-4} \text{ m}^2$, associated with the thin long arm, the inequality (3.4) is satisfied for $M = 10$. The arm is simulated by a chain of vertebrae grouped into two vertebra clusters, each cluster defining a tentacle segment.

Problem A. The measuring of the curvature is obtained by a distributed angle sensor network. A spatial weighting function, that satisfies the conditions (3.11)–(3.13), is selected for $\xi_0 = 0$, $\xi_1 = 0.5 \text{ m}$, $\xi_2 = 1.0 \text{ m}$. The eigenvalue Λ is evaluated as $\Lambda = 684$. We simulated two motion sequences. During the first sequence (Sequence 1, Fig. 6), the arm (both segments) is moving towards the desired position defined as

$$\left(\theta_i^d = \frac{\pi}{2} - i \frac{\pi}{14}, i = 1, 2, \dots, 24 \right)$$

or in term of curvature, $\kappa_{\theta d} = -\frac{\pi}{14}$.

A control law (4.2) with the controller gains, $k_{1\theta} = 20$, $k_{2\theta} = 8$ is used, where $k_{1\theta}$, $k_{2\theta}$ verifies the conditions (4.3), (4.4), (4.6). During the Sequence 2, the 1st segment is blocked and the 2nd segment is moved toward the desired curvature defined as

$$\left(\theta_i^d = i \frac{\pi}{14}, i = 13, 14, \dots, 24 \right) \text{ or } \kappa_{\theta d} = \frac{\pi}{14}.$$

Figures 6 and 7 report the arm evolutions during the two motion sequences. Figure 8 shows the error evolution during the Sequence 1 and Fig. 9 illustrates the Phase portrait of the Sequence 2.

Problem B. The measuring of the curvature is obtained by a curvature sensor placed at the end of the segment.

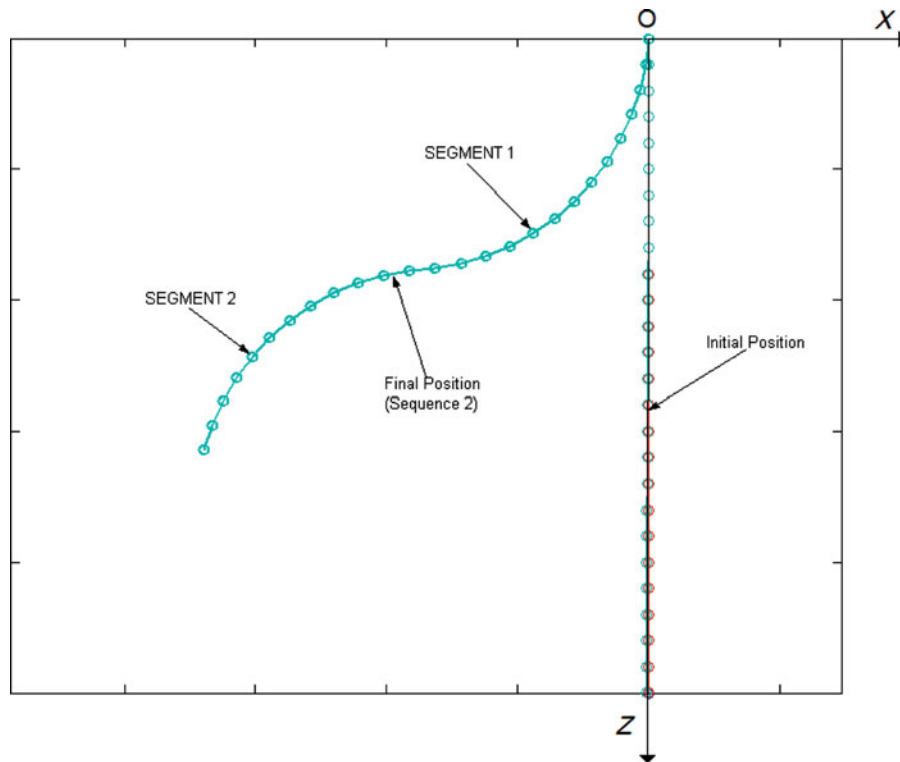


Fig. 7. The arm motion during the Sequence 2 (Problem A).

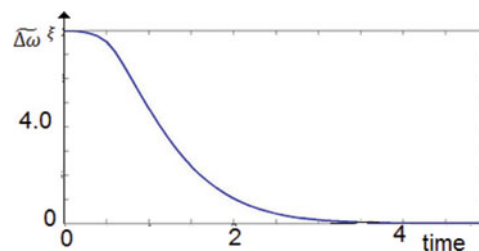


Fig. 8. The error evolution during the Sequence 1 (Problem A).

A 3-D control for a coiling motion of a load represented by a cylinder with the radius $r = 0.1$ is simulated. The coiling function is characterised by an objective function defined by the curvatures ($\kappa_{\theta d}(l) = 10$, $\kappa_{qd}(l) = 0.2$) with the boundary conditions $\kappa_{\theta d}(0) = 0$, $\kappa_{qd}(0) = 0$. A control algorithm (4.5) with $K_1 = \text{diag}(25, 15)$, $K_2 = \text{diag}(8, 4)$ is used. These control coefficients meet the conditions (4.6), (4.7). The evolution of the arm is illustrated in Fig. 10 and the phase portrait of the error dynamics is shown in Fig. 11. The good performances of the proposed control algorithm are derived from the graphs.

6. Experimental Results

In order to verify the suitability of the control algorithm, a platform with a tentacle arm was employed for testing. The arm consists of a chain of vertebrae, periodically spaced, each element having a special joint that ensures the rotation, elastic contact and the controllable friction force with the following element. All the joints are passive. All these elements determine a backbone type behaviour of the arm. The driving system of this arm is a hybrid one: a DC motor system with cable-tendons ensures the main motion of the arm and a pneumatic system controls the damping forces in the system joints. The motion of the arm, the bending, is determined by antagonistic cables (tendons) attached to the terminal point of the arm and that run through all the elements. These cables develop the driven forces.

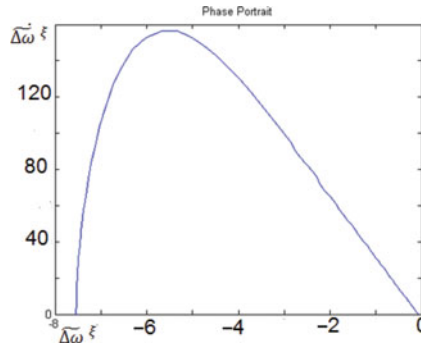


Fig. 9. The Error Phase Portrait of the Sequence 2 (Problem A).

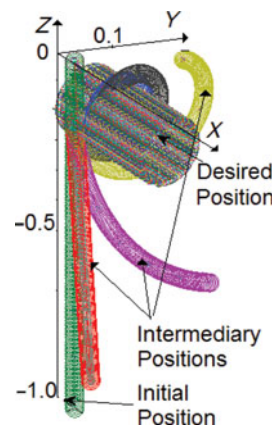


Fig. 10. The arm motion in the position control (Problem B).

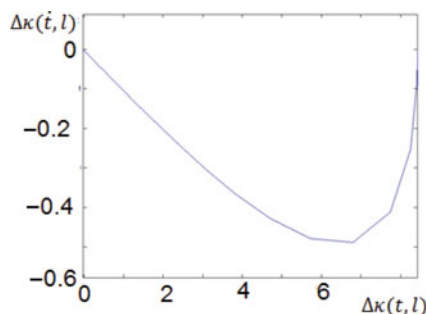


Fig. 11. The Error Phase Portrait (Problem B).

Figure 12 presents the configuration of such an element. Mainly, it consists of a spherical socket and a pivot. Because the cables do not drive every element, externally attached springs between elements are introduced between elements. The high flexibility of the arm is obtained by these rotational joints associated with the springs, distributed along the arm (Fig. 13). A pneumatic driven system composed by a single acting mini-cylinder is attached to each element. The cylinder develops a variable friction force in the i-joint. The elements of the arm are clustered in two segments, each segment having its own pneumatic control system. The level of the forces can be increased gradually which ensures a controllable value of the friction forces in all the joints. For high values of these forces, all the segment joints can be locked.

A polymer thick film layer is placed on the upper element of each segment without restricting the motion of the arm in the θ -plane. This sensor measures the curvature variable κ_θ in the θ -plane. The sensor exhibits a decrease in resistance when an increase of the film curvature is used. A Wheatstone

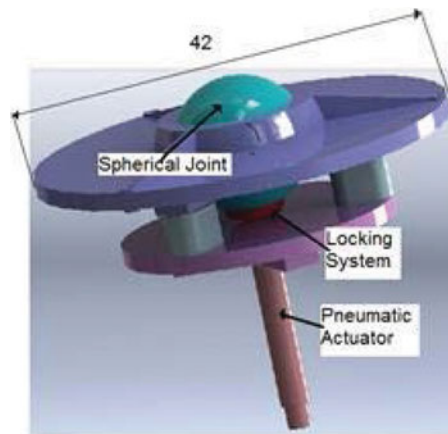


Fig. 12. The configuration of an element.

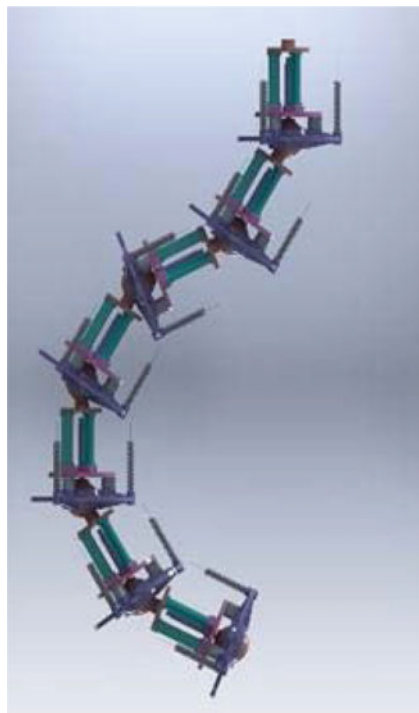


Fig. 13. The structure of the arm.

bridge system is used to measure the variation of the resistance. A Quanser based platform is used for the control and signal acquisition.

Figure 14(a) shows the arm in the initial position, i.e. a vertical one. A control law (4.5) with $\kappa_{\theta d} = 1.4 \text{ rad.m}^{-1}$ is implemented. Figure 14(b) presents the new position of the arm and Fig. 15 conveys the sensor information. Now, segment 1 is locked and a new actuation is obtained by bending the segment 2 for a new desired position $\kappa_{\theta d} = -2.25 \text{ rad.m}^{-1}$. This position is illustrated in Fig. 14(c) and the curvature error is presented in Fig. 16. The analysis of this experimental result re-confirms the algorithm performance.

7. Conclusions

The paper analyses the shape control problem for a class of hyper-redundant robot arms with continuum elements, a tentacle arm, characterized by an elastic backbone system. A sensor network

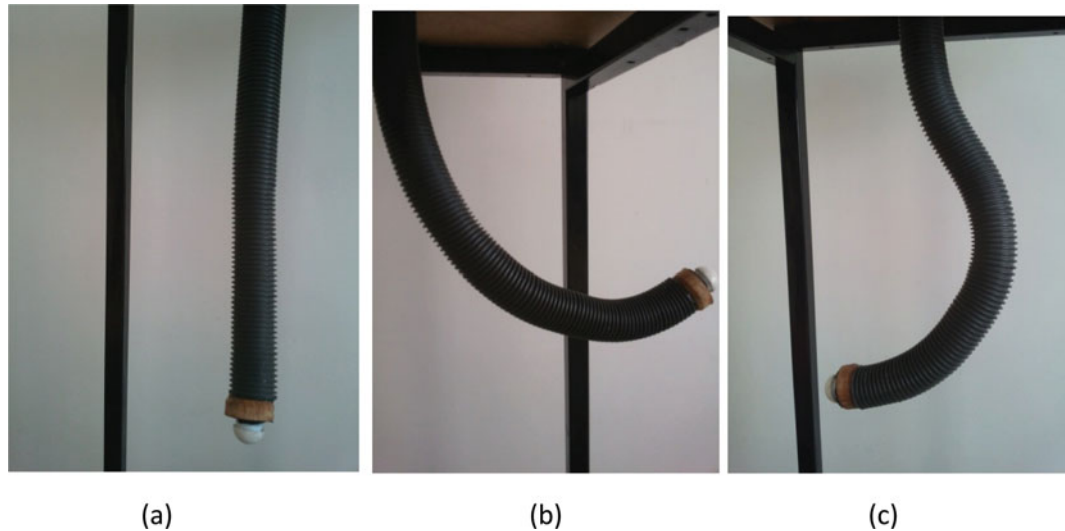


Fig. 14. The positions of the arm- experimental platform.

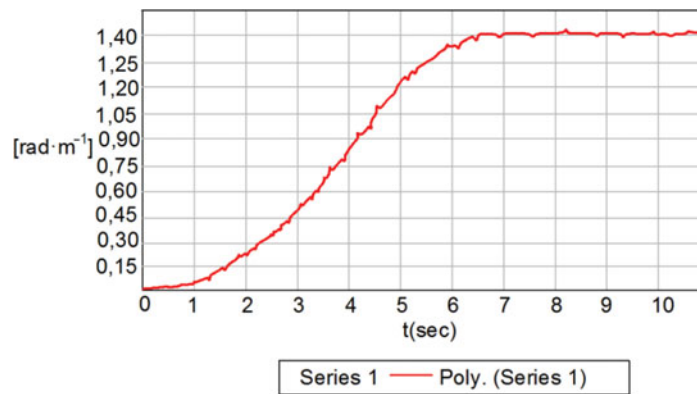


Fig. 15. The trajectory $\theta(t, \xi_1)$ - Segment Sensor 1.

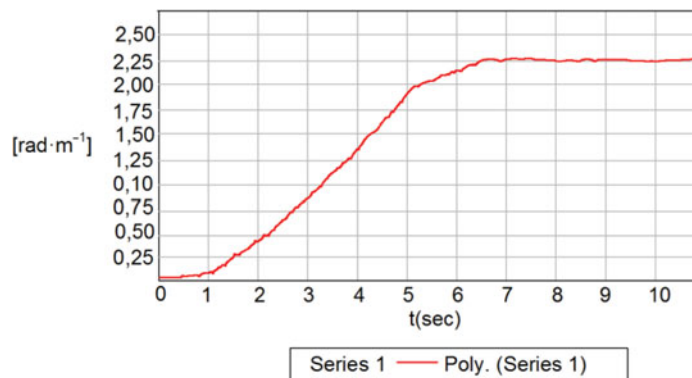


Fig. 16. The trajectory $\theta(t, \xi_N)$ - Segment Sensor 2.

distributed along the arm robot is used for the shape control. A spatial weighted technique for sensor measurements is used in order to facilitate the parameter estimation. The main parameters of the arm shape such as curvature and curvature gradient or the shape Jacobian associated with the control problem are estimated. Two measuring systems are used: a) a distributed angle sensor network and b) a curvature sensor placed at the end of the arm segment. The stability analysis and the resulting controllers are obtained using the concept of boundary geometric control and a weighted state control

method. This method transforms the infinite dimensional system associated with the arm model in a finite dimensional problem. The shape control algorithms for dynamic models with uncertain components are proposed. Theorem 1 provides a simple solution for the shape control of the tentacle models with distributed angle sensor network. Theorem 2 determines the control solutions using the dynamic model expressed in terms of curvature parameters. Numerical simulations and experimental results illustrate the effectiveness of the presented algorithms and techniques.

Acknowledgements

This work was supported by the PCCA 150/2012 grant of the Executive Agency for Higher Education, Research, Development and Innovation Funding (UEFISCDI).

References

1. G. Robinson and J. B. C. Davies, "Continuum Robots – A State of the Art," *Proceedings of the IEEE International Conference on Robotics and Automation*, Detroit, May 1999, pp. 2849–2854.
2. G. S. Chirikjian and J. W. Burdick, "Design and Experiments with a 30 DOF Robot," *Proceedings of the IEEE International Conference on Robotics and Automation* (1993) pp. 113–119.
3. G. S. Chirikjian and J. W. Burdick, "Kinematics of Hyper-Redundant Robot Locomotion with Applications to Grasping," *Proceedings of the IEEE International Conference Robotics and Automation* (1991) pp. 720–725.
4. G. S. Chirikjian and J. W. Burdick, "An Obstacle Avoidance Algorithm for Hyper-Redundant Manipulators," *Proceedings of the IEEE International Conference on Robotics and Automation*, Cincinnati, Ohio (May 1990) pp. 625–631.
5. G. S. Chirikjian, "Hyper-redundant manipulator dynamics: A continuum approximation," *Adv. Robot.* **9**(3), 217–243 (1995).
6. I. A. Gravagne and Ian D. Walker, "On the Kinematics of Remotely - Actuated Continuum Robots," *Proceedings of the IEEE International Conference on Robotics and Automation*, San Francisco, (April 2000), pp. 2544–2550.
7. I. A. Gravagne and Ian D. Walker, "Uniform Regulation of a Multi-Section Continuum Manipulators," *Proceedings of the IEEE International Conference on Robotics and Automation*, Washington DC, (May 2002), pp. 1519–1525.
8. H. Mochiyama and H. Kobayashi, "The Shape Jacobian of a Manipulator with Hyper Degrees of Freedom," *Proceedings of the IEEE International Conference on Robotics and Automation*, Detroit, (May 1999), pp. 2837–2842.
9. D. Braganza, D. M. Dawson, I. D. Walker and N. Nath, "A neural network controller for continuum robots," *IEEE Trans. Robot.* **23**(6), 1270–1277 (Dec. 2007).
10. I. Walker and M. Hannan, "A novel elephant's trunk robot," *Proceedings of IEEE/ASME International on Advanced Intelligent Mechatronics 1999*, Atlanta, USA, (Sep. 19–23, 1999) pp. 410–415.
11. B. Jones and I. D. Walker, "Practical kinematics for real-time implementation of continuum robots," *IEEE Trans. Robot.* **22**(6), 1087–1099 (Dec. 2006).
12. A. Kapadia, I. Walker and D. Dawson, "A Model – Based Sliding Mode Controller for Extensible Continuum Robots," *Recent Advances in Signal Processing, Robotics and Automation*, ISPRA Conf., (2009), pp. 103–120.
13. D. C. Rucker, R. J. Webster, III, G. S. Chirikjian and N. J. Cowan, "Equilibrium Conformations of Concentric-Tube Continuum Robots," *Int. J. Robot. Res.* **29**(10), 1263–1280 (2010).
14. I. Gravagne and I. D. Walker, "Manipulability and Force Ellipsoids for Continuum Robot Manipulators," *IEEE/RSJ International Conference on Intelligent Robots and Systems*, Maui, Hawaii, (Oct 29–31, 2001), pp. 304–310.
15. M. Ivanescu, N. Bizdoaca, M. Florescu, N. Popescu and D. Popescu, "Frequency Criteria for the Grasping Control of a Hyper-redundant Robot," *Proceedings of the IEEE International Conference on Robotics and Automation*, Anchorage, Alaska (ICRA 2010), (May 3–8, 2010), pp. 1542–1549.
16. M. Ivanescu, D. Cojocaru, N. Bizdoaca, M. Florescu, N. Popescu, D. Popescu and S. Dumitru, "Boundary control by boundary observer for hyper-redundant robots," *Int. J. Comput. Commun. Control* **755–767** (2010).
17. G. La Spina, M. Sfakiotakis, D. Tsakiris, A. Memciassi and P. Dario, "Polychaete-Like undulatory robotic locomotion in unstructured substrates," *IEEE Trans Robot.* **23**(6), 1200–1212 (Feb 2007).
18. Ke Jun Ning and F. Worgotter, "A novel concept for building a hyper-redundant chain robot," *IEEE Trans Robot.* **25**(6), 1237–1248 (Dec 2009).
19. D. C. Rucker, B. A. Jones and R. J. Webster, III, "A geometrically exact model for externally loaded concentric-tube continuum robots," *IEEE Trans Robot.* **26**(5), 769–780 (Oct 2010).
20. Y. Bailly, Y. Amirat and G. Fried, "Modeling and control of a continuum style microrobot for endovascular surgery," *IEEE Trans Robot.* **27**(5), 1024–1030 (Oct 2011).

21. A. Bajo, N. Simaan, "Kinematics-based detection and localization of contacts along multisegment continuum robots," *IEEE Trans Robot.* **28**(2), 291–302 (April 2012).
22. D. Trivedi, C. D. Rahn, W. M. Kier and I. D. Walker, "Soft robotics; Biological inspiration, state of art and future research," *Appl. Bionics Biomechan.* **5**(3), 99–117 (2008).
23. S. Hirose, *Biologically Inspired Robots: Snake-Like Locomotors and Manipulators* (Oxford University Press, Oxford, UK, 1993).
24. H. Choset, K. M. Lynch, S. Hutchinson, G. Kantor, W. Burgard, L. E. Kavraki and S. Thrun, *Principles of Robot Motion, Theory, Algorithms and Implementations* (MIT Press, Boston, 2005).
25. Shugen Ma, Naoki Tadokoro, and Kousuke Inoue, "Influence of gradient of a slope to optimal locomotion curves of a snake-like robot," *Int. J. Adv. Robot.* **20-4**, 413–428 (2006).
26. B. A. Jones and I. D. Walker, "Kinematics for multisection continuum robots," *IEEE Trans. Robot.* **22**(1), 43–51 (Feb. 2006).
27. R. Fareh, M. Saad and M. Saad, "Workspace Tracking Trajectory for 7-DOF ANAT Robot using a Hierarchical Control Strategy," *20th Mediterranean Conference on Control & Automation (MED)*, Barcelona, Spain, (July 3–6, 2012), 122–128.
28. H. Shang, J. F. Forbes and M. Guay, "Feedback Control of Hyperbolic Distributed Parameter Systems," *Chem. Eng. Sci.* **60**, 969–980 (2005).
29. A. Maida, J. P. Corriou, "Boundary Control of Nonlinear Distributed Parameter Systems by Input-Output Linearization," *18th IFAC Congress*, Milano, (Aug. 228–30), 10910–10916.
30. F. Fahimi, H. Ashrafiuon and C. Nataraj, "An improved inverse kinematic and velocity solution for spatial hyper-redundant robots," *IEEE Trans. Robot. Automat.* **18**(1), 103–107 (Feb. 2002).
31. S. Hirose, and Y. Umetani, "Kinematic Control of Active Cord Mechanism With Tactile Sensors," *Proceedings of the 2nd Int CISM-IFT Symp. On Theory and Practice of Robots and Manipulators* (1976), pp. 241–252.
32. A. Kapadia, I. Walker and D. Dawson, "A Model – Based Sliding Mode Controller for Extensible Continuum Robots," *Recent Advances in Signal Processing, Robotics and Automation, ISPRA Conf.*, (2009), pp. 103–120.
33. R. J. Webster and B. A. Jones, "Design and kinematic modelling of constant curvature continuum robots: A review," *Int. J. Robot. Res.* **29**(13), 1661–1683 (2010).
34. M. W. Hannan, "Real-time estimation for continuum robots using vision," *Robotica* **23**(05), 645–661 (Sept. 2005).
35. D. Camarillo and C. Milne, "Mechanics modeling of tendon – driven continuum manipulators," *IEEE Trans. Robot.* **24**(6), 1262–1273 (December 2008).
36. S. Sareh, J. Rossiter, A. Conn, K. Drescher and R. Goldstein, "Swimming like algae: biomimetics soft artificial cilia," *J.R. Soc. Interface*, 621–634 (2012).
37. Y. Orlov, A. Pissano and E. Usai, "Exponential stabilization of the uncertain wave equation via distributed dynamic input extension," *IEEE Trans. Aut. Control* **56**(1), 212–218 (2011).
38. F. P. Beer and E. R. Johnston, Jr, *Mechanics of Materials* (McGraw-Hill, New York, 1981).
39. R. Schilling, *Fundamental of Robotics* (Prentice Hall, 1990).

APPENDIX 1

We consider the Jacobian

$$J = \begin{bmatrix} J_{11} & J_{12} \\ J_{21} & J_{22} \end{bmatrix} \quad (\text{A1.1})$$

where

$$J_{11} = \frac{d\eta_1}{d\tilde{\theta}^\xi} = \frac{d\eta_1}{d\kappa_\theta} \cdot \frac{d\kappa_\theta}{d\tilde{\theta}^\xi}$$

From (3.33), (3.34), we have

$$\Delta\kappa = \int_0^s \Delta\kappa' ds + \Delta\kappa(0).$$

The initial condition $\Delta\kappa(0) = 0$, in (3.29) yields

$$J_{11} = -(\kappa_\theta - \kappa_{\theta d}) \int_0^l \frac{1}{(EI)_\theta} \left(c_\theta + \frac{d\tilde{h}_1}{d\tilde{\theta}} \right) ds. \quad (\text{A1.2})$$

A similar procedure results in

$$J_{12} = 0, \quad (\text{A1.3})$$

$$J_{21} = 0, \quad (\text{A1.4})$$

$$J_{22} = -(\kappa_q - \kappa_{qd}) \int_0^l \frac{1}{(EI)_q} \left(c_q + \frac{d\tilde{h}_2}{d\tilde{q}} \right) ds. \quad (\text{A1.5})$$

APPENDIX 2

Let us consider the Liapunov function

$$V = V(t) = \frac{1}{2} \Delta \dot{\omega}^\xi(t)^T I_\rho \Delta \dot{\omega}^\xi(t) + \frac{1}{2} \Delta \dot{\omega}^\xi(t)^T (EI\Lambda - C) \Delta \dot{\omega}^\xi(t) + \alpha \Delta \dot{\omega}^\xi(t) I_\rho \Delta \dot{\omega}^\xi(t), \quad (\text{A2.1})$$

where α is a positive constant that satisfies the condition

$$4I_\rho (EI\Lambda - C) - \alpha^2 \mathbf{I} > 0. \quad (\text{A2.2})$$

The function V can be rewritten as

$$V = \frac{1}{2} \begin{bmatrix} \Delta \dot{\omega}^\xi \\ \Delta \dot{\omega}^\xi \end{bmatrix}^T P \begin{bmatrix} \Delta \dot{\omega}^\xi \\ \Delta \dot{\omega}^\xi \end{bmatrix}, \quad (\text{A2.3})$$

where

$$P = \begin{bmatrix} I_\rho \alpha I_\rho \\ \alpha I_\rho (EI\Lambda - C) \end{bmatrix} \quad (\text{A2.4})$$

and the condition (A2.2) ensures that V is positive definite. Taking the derivative of V ,

$$\dot{V} = \Delta \dot{\omega}^\xi T I_\rho \ddot{\Delta \omega}^\xi + \ddot{\Delta \omega}^\xi T (EI\Lambda - C) \dot{\Delta \omega}^\xi + \alpha \dot{\Delta \omega}^\xi T I_\rho \ddot{\Delta \omega}^\xi + \alpha \dot{\Delta \omega}^\xi T I_\rho \ddot{\Delta \omega}^\xi \quad (\text{A2.5})$$

and substituting (3.13), it follows that,

$$\begin{aligned} \dot{V} = & -\dot{\Delta \omega}^\xi T (B - \alpha I) \dot{\Delta \omega}^\xi - \alpha \ddot{\Delta \omega}^\xi T B \dot{\Delta \omega}^\xi - \alpha \ddot{\Delta \omega}^\xi T (EI\Lambda - C) \dot{\Delta \omega}^\xi \\ & + \dot{\Delta \omega}^\xi T \left(\ddot{\Delta h} + \frac{\chi(l, \xi)}{\chi(\xi)} \Delta \tau \right) + \alpha \ddot{\Delta \omega}^\xi T \left(\left(\ddot{\Delta h} + \frac{\chi(l, \xi)}{\chi(\xi)} \Delta \tau \right) \right) \end{aligned} \quad (\text{A2.6})$$

where in order to simplify the notation, the time variable t was omitted.

By evaluating (A2.6) along the solutions of (3.1) and taking into account the inequalities (3.4), after simple additional manipulations, we have

$$\dot{V} \leq - \begin{bmatrix} \dot{\Delta \omega}^\xi \\ \ddot{\Delta \omega}^\xi \end{bmatrix}^T Q \begin{bmatrix} \dot{\Delta \omega}^\xi \\ \ddot{\Delta \omega}^\xi \end{bmatrix}, \quad (\text{A2.7})$$

where

$$Q = \begin{bmatrix} (B - \alpha I + K_2) \frac{1}{2} (\alpha B - (MI - K_1) - \alpha (MI - K_2)) \\ \frac{1}{2} (\alpha B - (MI - K_1) - \alpha (MI - K_2)) \alpha (EI\Lambda - C) + \alpha K_1 \end{bmatrix}. \quad (\text{A2.8})$$

Taking into account the conditions (4.3),(4.4), Q is positive definite. Also, the inequality (A2.7) can be rewritten as the following differential inequality

$$\dot{V} \leq -\frac{\lambda_{\min}(Q)}{\lambda_{\max}(P)} \left[\begin{array}{c} \dot{\tilde{\Delta}}\omega\xi \\ \tilde{\Delta}\omega\xi \end{array} \right]^T P \left[\begin{array}{c} \dot{\tilde{\Delta}}\omega\xi \\ \tilde{\Delta}\omega\xi \end{array} \right] = -\frac{\lambda_{\min}(Q)}{\lambda_{\max}(P)} V, \quad (\text{A2.9})$$

where $\lambda_{\min}(Q)$, $\lambda_{\max}(P)$ are the minimum and maximum eigenvalues of the matrices, Q and P . This relation proves that the exponential convergence of $\frac{\dot{\tilde{\Delta}}\omega\xi}{\tilde{\Delta}\omega\xi}$ to zero as $t \rightarrow \infty$. Taking into account (3.41), it yields

$$\lim_{t \rightarrow \infty} \Delta\eta = 0 \quad (\text{A2.10})$$

or

$$\kappa_{\theta} \rightarrow \kappa_{\theta d} \text{ and } \kappa_q \rightarrow \kappa_{qd}$$

and

APPENDIX 3

In the case of this control problem, we use the dynamic model (3.47). The desired curvature vector $\kappa_d(l)$ is derived from the equation,

$$\frac{1}{2}l^2 C\kappa'_d + h(\kappa'_d, l) + \frac{1}{l}\tau_d = 0 \quad (\text{A3.1})$$

and

$$\kappa_d(l) = \kappa_d(0) + \kappa'_d l, \quad (\text{A3.2})$$

$$\kappa(t, 0) = \kappa_d(0), \quad (\text{A3.3})$$

$$\Delta\kappa(t) = \kappa_d(l) - \kappa(t, l), \quad (\text{A3.4})$$

$$\Delta\tau(t) = \tau_d - \tau(t). \quad (\text{A3.5})$$

we introduce a Liapunov function

$$V = \left[\begin{array}{c} \Delta\kappa(i, l) \\ \Delta\kappa(t, l) \end{array} \right]^T P \left[\begin{array}{c} \Delta\kappa(i, l) \\ \Delta\kappa(t, l) \end{array} \right] \quad (\text{A3.6})$$

with

$$P = \left[\begin{array}{cc} \frac{l}{2}I_{\rho} \alpha \frac{l}{4}I_{\rho} \\ \alpha \frac{l}{4}I_{\rho} \frac{l}{2}C \end{array} \right]. \quad (\text{A3.7})$$

The condition (4.8) ensures that P is a positive definite matrix. Using the same procedure as with Theorem 1, it follows that,

$$\dot{V} \leq - \left[\begin{array}{c} \Delta\kappa(i, l) \\ \Delta\kappa(t, l) \end{array} \right]^T Q \left[\begin{array}{c} \Delta\kappa(i, l) \\ \Delta\kappa(t, l) \end{array} \right] \quad (\text{A3.8})$$

where, taking into account the conditions (4.6), (4.7), Q is positive definite. This inequality can be rewritten as

$$\dot{V} \leq -\frac{\lambda_{\min}(Q)}{\lambda_{\max}(P)} \begin{bmatrix} \Delta\kappa(i, l) \\ \Delta\kappa(t, l) \end{bmatrix}^T P \begin{bmatrix} \Delta\kappa(i, l) \\ \Delta\kappa(t, l) \end{bmatrix} = -\frac{\lambda_{\min}(Q)}{\lambda_{\max}(P)} V \quad (\text{A3.9})$$

which proves the exponential convergence of $\frac{\Delta\kappa(i, l)}{\Delta\kappa(t, l)}$ to zero,

$$\lim_{t \rightarrow \infty} \frac{\Delta\kappa(i, l)}{\Delta\kappa(t, l)} = 0. \quad (\text{A3.10})$$